Supporting Information

Enhancing the Separation of C_2H_4/C_2H_6 in Customized MOR Zeolite

Hongwei Chen,[†a] Binyu Wang,[†b] Bin Zhang,[†c] Yongheng Ren,[a] Jiuhong Chen,[a] Jiabao Gui,[a] Xiufeng Shi,[c] Wenfu Yan,[b] Jinping Li,[a] and Libo Li[*a]

a College of Chemical Engineering and Technology, State Key Laboratory of Clean and Efficient Coal Utilization, Taiyuan University of Technology, Taiyuan 030024, China.
b State Key Laboratory of Inorganic Synthesis and Preparative Chemistry, College of Chemistry, Jilin University, 2699 Qianjin Street, Changchun 130012, China.
c College of Chemistry, Taiyuan University of Technology, Taiyuan 030024, China.

*Corresponding Author.
†These authors contributed equally.

E-mail: lilibo@tyut.edu.cn (Libo Li)

This Supporting Information Includes:

Details for experiments, characterizations and calculations

Tables S1-S5

Figures S1-S25

Table S1. Reagents information.

Name	Chemical formula	Manufacturer	Purity	Mass
Silica sol	SiO_2	JALON Micro-nano New Materials Co., Ltd	30wt%	30 kg
Sodium hydroxide	NaOH	China National Pharmaceutical Group Corporation	AR	500 g
Sodium aluminate	$NaAlO_2$	China National Pharmaceutical Group Corporation	AR	500 g
Deionized water	H_2O	China National Pharmaceutical Group Corporation	-	25 kg
COM-MOR	MOR	Tianjin Yuanli Chemical Co., LTD	>99%	100 g

Table S2. The information of the samples synthesized.

Sequence	Feed Gel Si/Al	$NaAlO_2$	Product	Crystallinity %	Product Si/Al[a]	Product Si/Al[b]
1	22.88	0.25375	AM	0	-	-
2	19.07	0.3045	AM	0	-	-
3	16.34	0.35525	AM	0	-	-
4	14.3	0.406	AM+MOR	31.5	-	-
5	12.71	0.45675	MOR	78.6	12.1	9.15
6	11.44	0.5075	MOR	79.7	10.1	8.47
7	10.4	0.55825	MOR	81.2	8.6	6.56
8	9.53	0.609	MOR	81.6	7.53	6.10
9	8.17	0.7105	MOR	81.5	6.74	5.78
10	7.15	0.812	MOR	80.6	6.21	5.02
11	6.36	0.9135	MOR	80.5	5.2	4.54
12	5.72	1.015	MOR	78.9	5.04	4.31
13	5.20	1.1165	MOR	75.1	4.87	3.78
14	4.58	1.26875	AM-MOR	52.7	-	-
15	3.81	1.5225	AM	33.8	-	-
16	2.86	2.03	AM	16.2	-	-

[AM] Amorphous forms. [a]: ICP elemental analysis. [b]: EDS spectral analysis.

$$Crystallinity = \frac{Area\ of crystalline\ peak}{Area\ of\ all\ peaks\ (crystalline + Amorphous)} \times 100$$

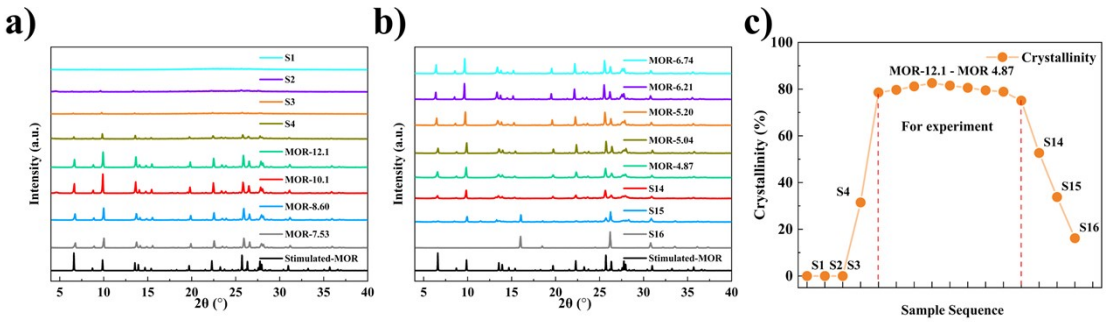

Fig. S1. (a-b) Simulated XRD pattern and experimental XRD patterns of MOR synthesized, (c) Crystallinity of samples.

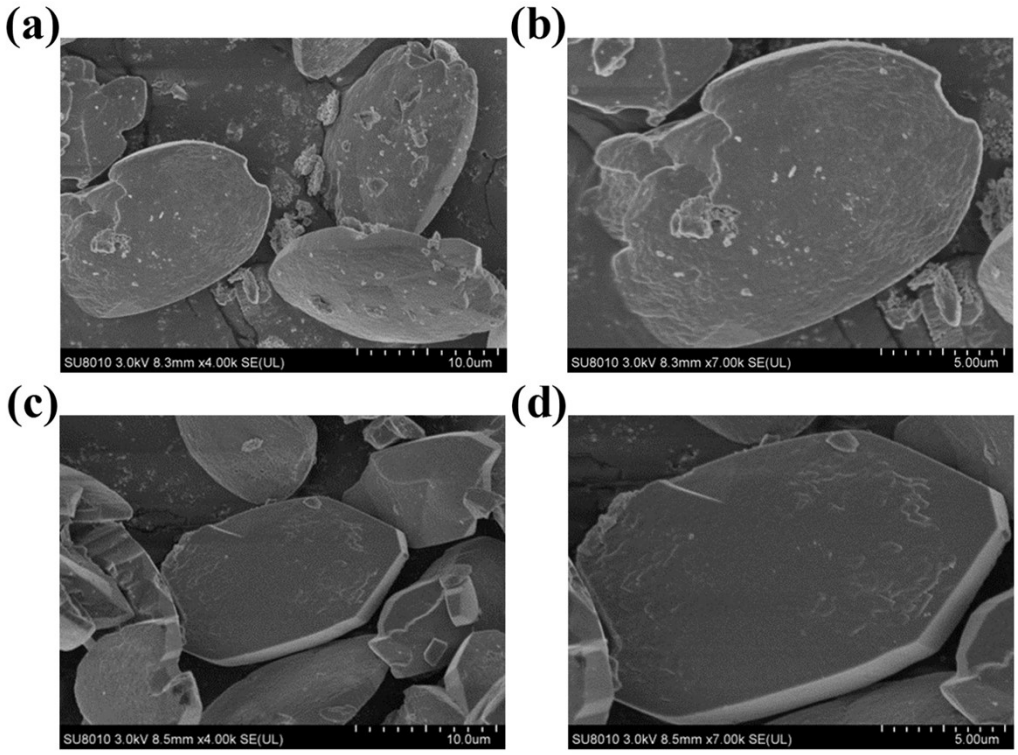

Fig. S2. The SEM images of (a-b) MOR-12.1 and (c-d) MOR-10.1.

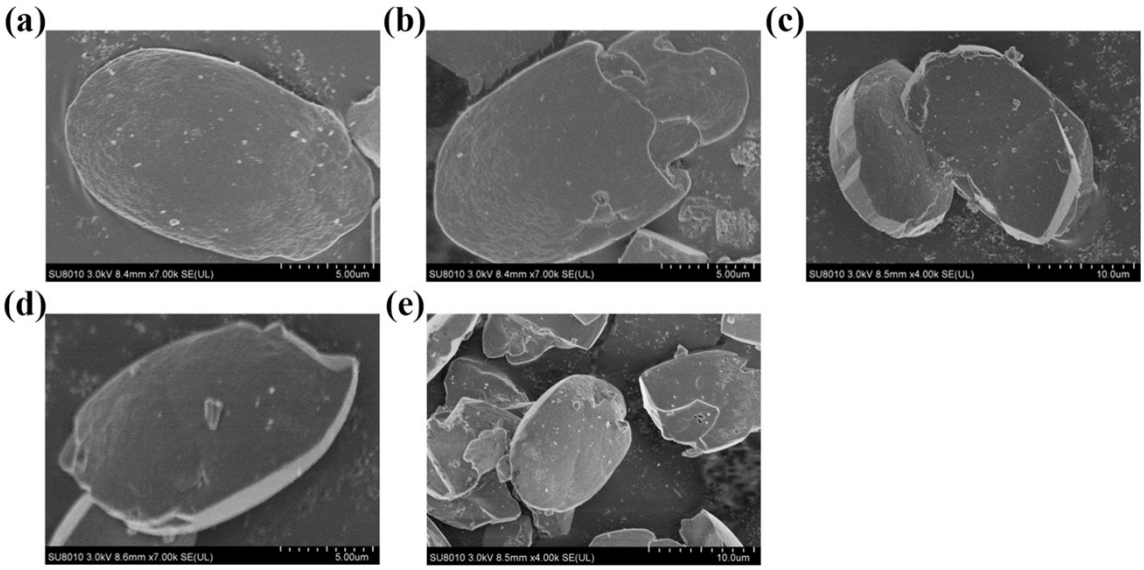

Fig. S3. The SEM images of (a) MOR-8.6, (b) MOR-7.5, (c) MOR-6.7, (d) MOR-5.2 and (e) MOR-4.8.

Thermogravimetric analysis

Thermal stability was evaluated by conducting thermogravimetric (**TG**) analysis on an STA449F5 instrument with a constant flow of nitrogen, while the sample was heated at a rate of 10 K/min.

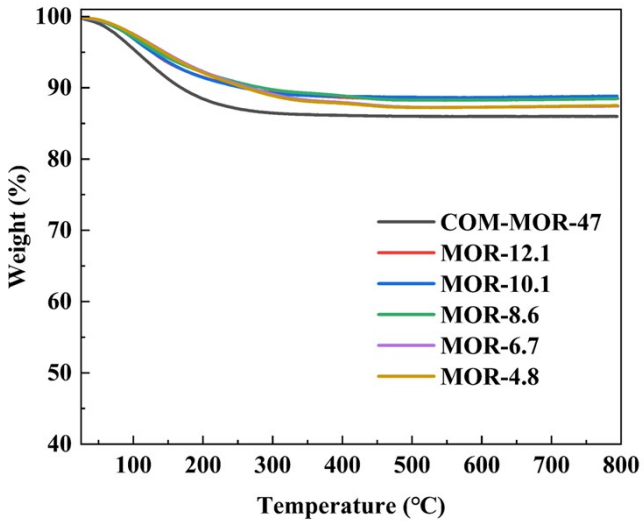

Fig. S4. TG curves.

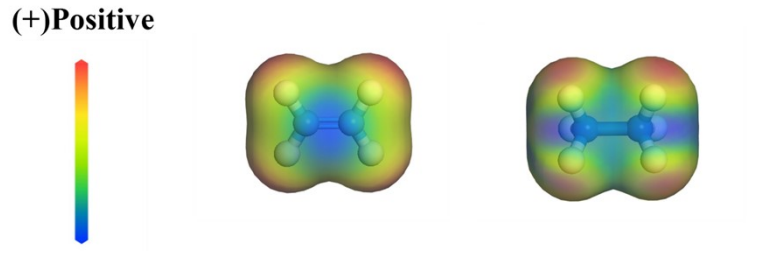

	C_2H_6	C_2H_4
Size (Å^3)	3.81 × 4.08 × 4.82	3.28 × 4.18 × 4.84
Kinetic diameter (Å)	4.44	4.2
Boiling point (K)	184.4	194.7

Fig. S5. Information of guest molecules and electrostatic potential distribution.

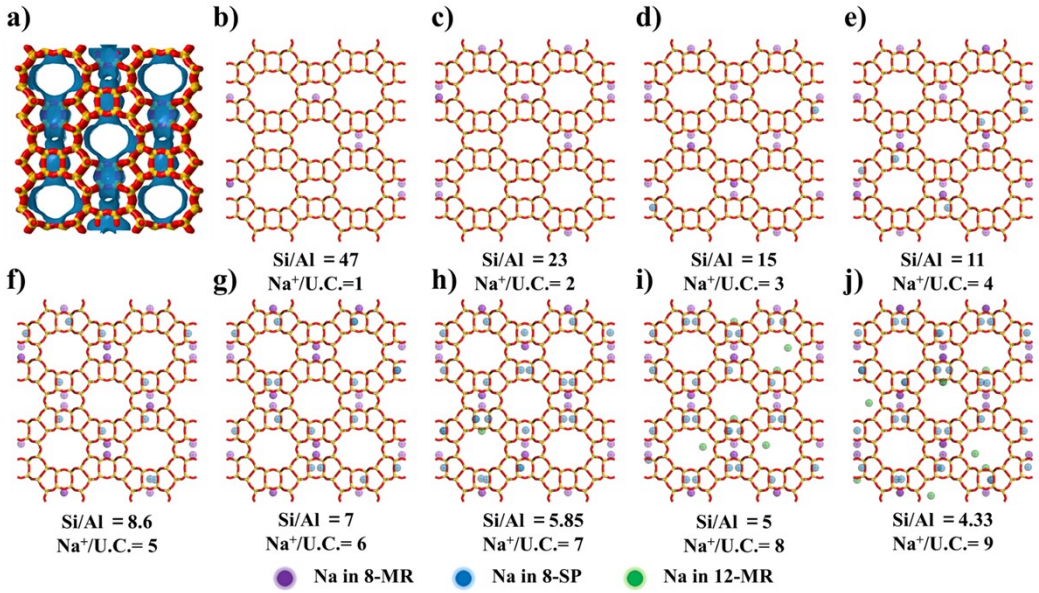

Fig. S6. (a) Diffusion channel system of MOR zeolite, (b-j) Na^+ cations distribution in MOR-*x*.

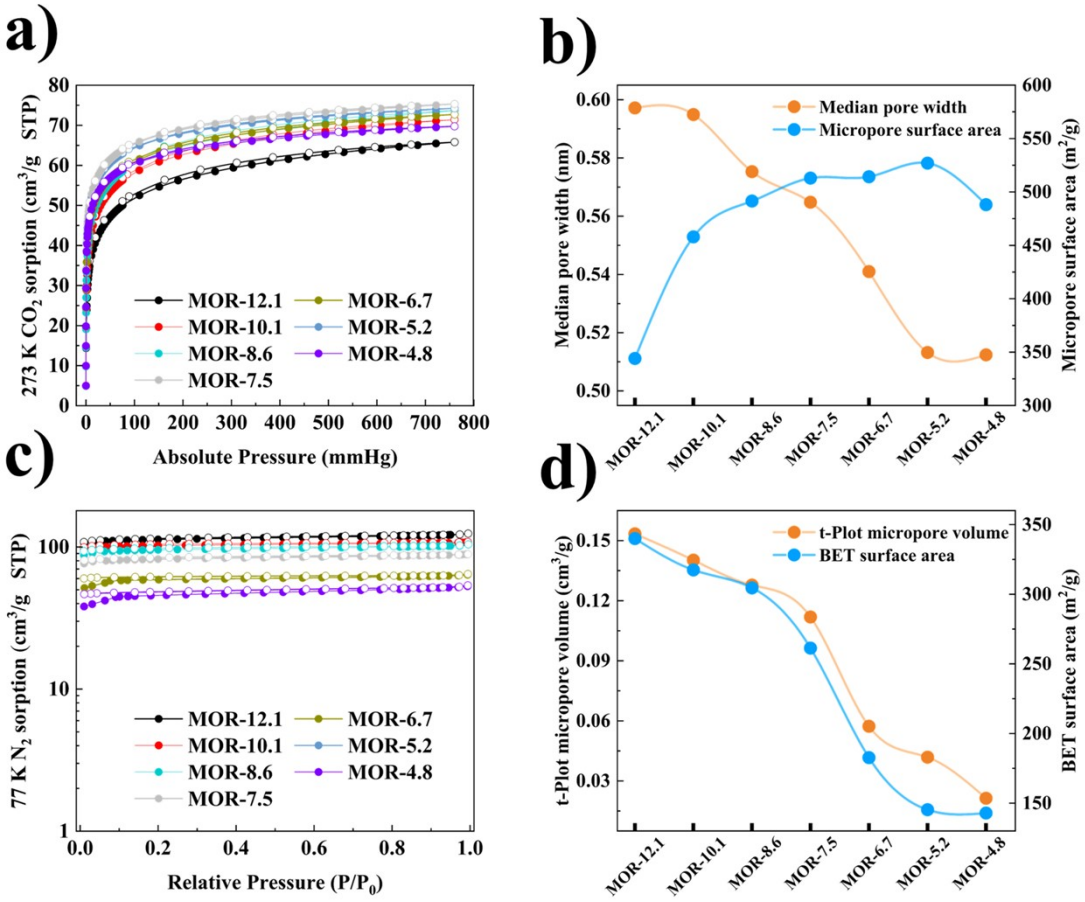

Fig. S7. (a, c) 273 K CO_2 and 77 K N_2 adsorption isotherms of MOR-*x*, (b) Median pore width and micropore surface area of MOR-*x*, (d) the specific surface area and micropore volume of MOR-*x*.

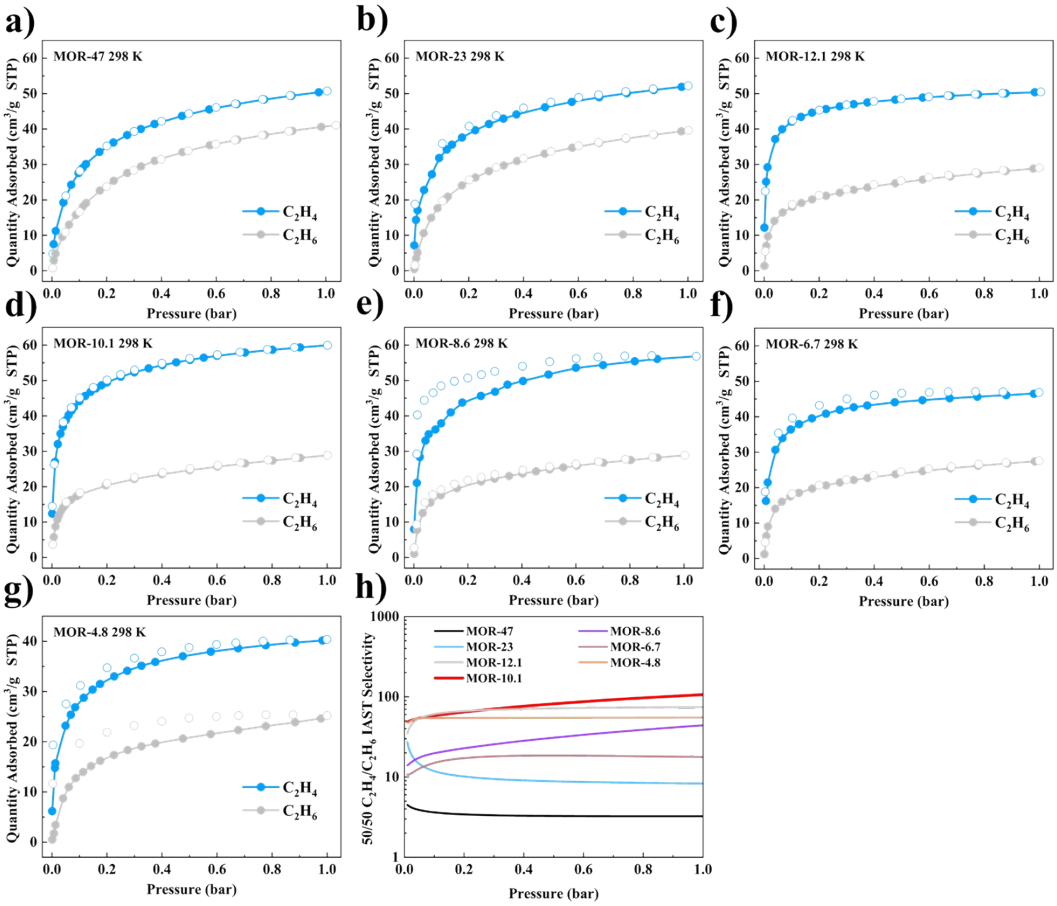

Fig. S8. (a-g) Single component adsorption isotherms of C_2H_4, and C_2H_6 on MOR-*x* at 298 K**,** (h) IAST selectivity for MOR-*x*.

Dual-site Langmuir-Freundlich isotherm model

The sorption of C_2H_4 and C_2H_6 was described using a Dual-site Langmuir- Freundlich isotherm model, which is formulated as:

$$q = \frac{q_c \times k_c \times P^{n_c}}{1 + k_c \times P^{n_c}} + \frac{q_i \times k_i \times P^{n_i}}{1 + k_i \times P^{n_i}}$$

The model involves parameters such as q_c (cm^3 g^{-1}) and q_i (cm^3 g^{-1}), which represent the saturation capacities of sites *c* and *i*; as well as k_c and k_i, which are the corresponding adsorption equilibrium constants that reflect the affinity coefficients of sites *c* and *i*, respectively. The model is based on the equilibrium pressure, which is denoted as *P*.

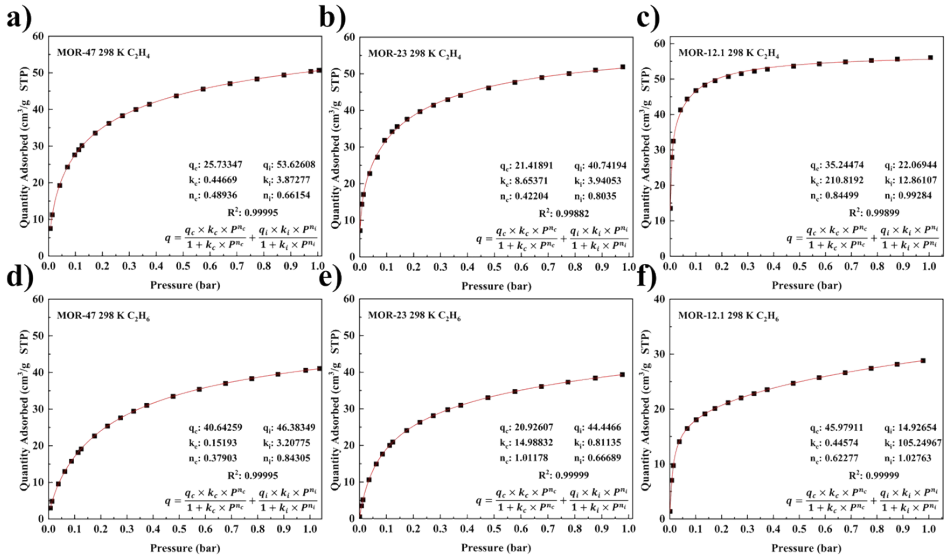

Fig. S9. (a-f) Non-linear fitted curves for C_2H_4 and C_2H_6 adsorption isotherms of MOR-*x* (*x* = 47, 23, and 12.1).

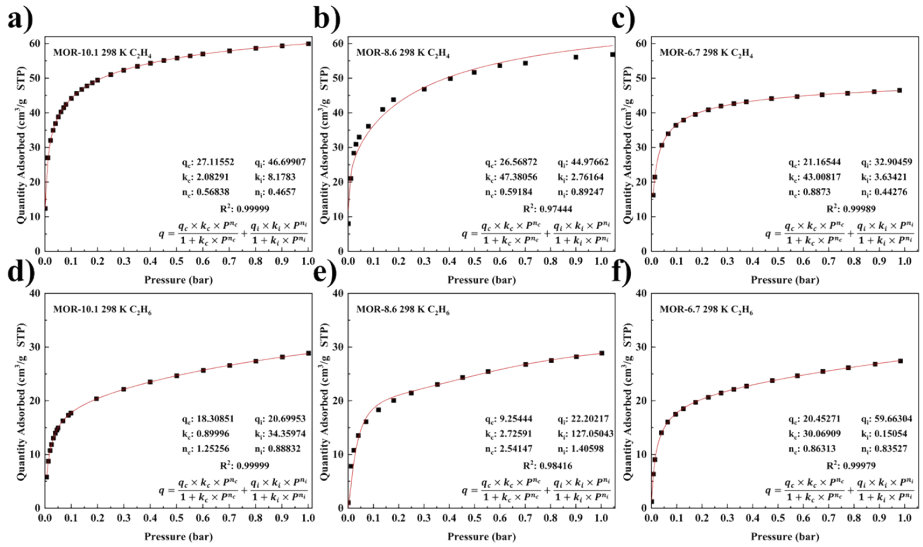

Fig. S10. (a-f) Non-linear fitted curves for C_2H_4 and C_2H_6 adsorption isotherms of MOR-*x* (*x* = 10.1, 8.6, and 6.7).

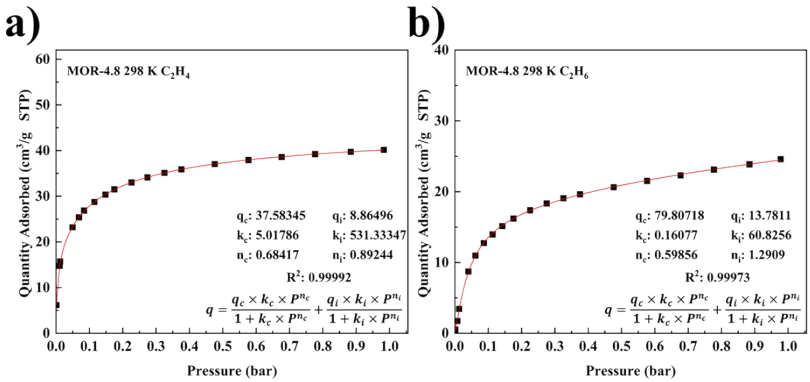

Fig. S11. (a-d) Non-linear fitted curves for C_2H_4 and C_2H_6 adsorption isotherms of MOR-4.8.

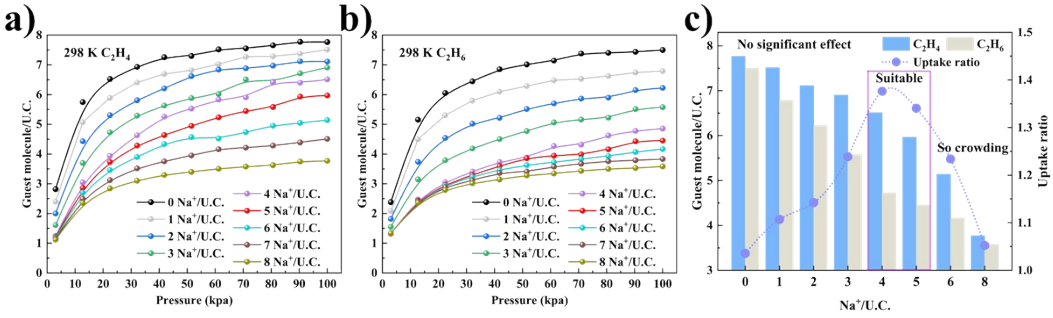

Fig. S12. Prediction of (a) C_2H_4 and (b) C_2H_6 adsorption isotherms, and (c) uptake ratio of MOR-*x*.

Table S3. Performance of inorganic adsorbents for C_2H_4/C_2H_6 (50/50) separation.

Adsorbent	C_2H_4 adsorbed (mmol g^{-1})	Selectivity	Reference
ITQ-55	1.5	~100	1
Na-ETS-10	2.04	4.7	2
Ag/SBA-15	0.76	5.27	3
Cu-MCM-48	0.49	3.80	4
CuCl@HY	2.14	67	5
CuCl/NaX	1.90	3.57	6
ITQ-29	1.33	1.66	7
MOR-46	2.26	3.24	This work
MOR-23	2.33	8.30	This work
MOR-12.1	2.25	58.63	This work
MOR-10.1	**2.67**	**106.39**	**This work**
MOR-8.6	2.53	44.06	This work
MOR-6.7	2.09	17.75	This work
MOR-4.8	1.80	16.78	This work

Isosteric heat of adsorption (Q_{st})

Isotherms for C_2H_4, and C_2H_6 sorption were measured at 298 K and 323 K, these isotherms were fitted to the virial equation:

$$\ln P = \ln N + \frac{1}{T}\sum_{i=0}^{m} a_i N^i + \sum_{i=0}^{n} b_i N^i$$

Where N is the amount of gas adsorbed at the pressure P, a and b are virial coefficients, m and n are the number of coefficients require to adequately describe the isotherm. To calculate the Q_{st} values, the fitting parameters obtained from equation were then plugged into the following equation:

$$Q_{st} = -R\sum_{i=0}^{m} a_i N^i$$

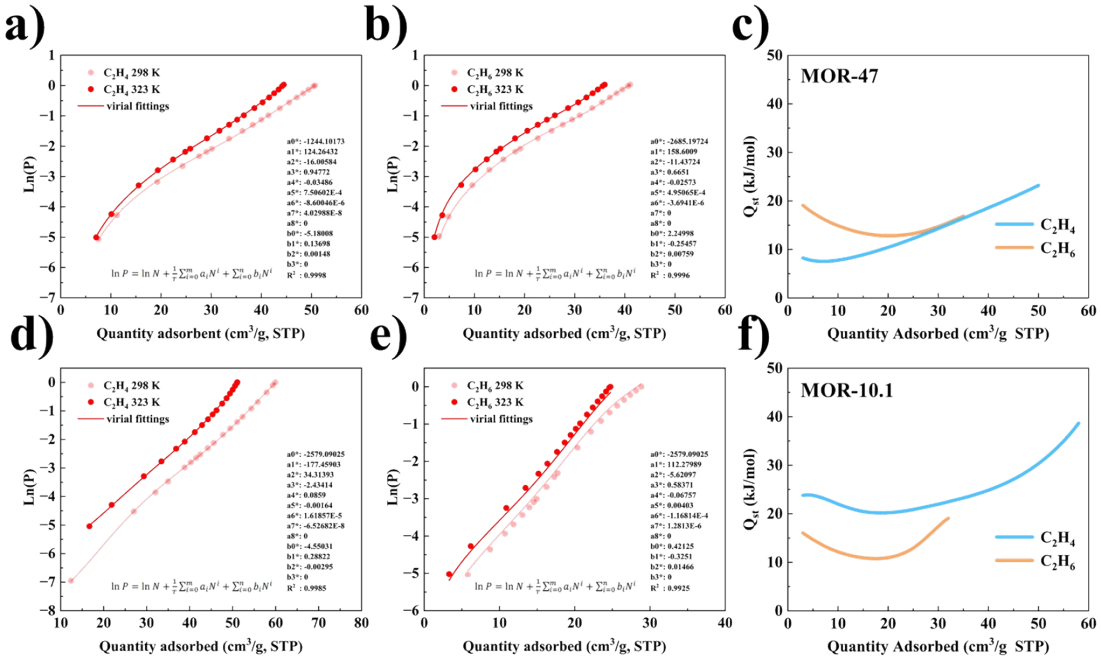

Fig. S13. Virial fitting of (a, d) C_2H_4, and (b, e) C_2H_4 adsorption isotherms of MOR-10.1 and 47, (c, f) Isosteric heats of adsorption of C_2H_4, and C_2H_6 of MOR-10.1 and 47.

Diffusional time constants

Diffusional time constants (D', D/r^2) were calculated by the short-time solution of the diffusion equation assuming a step change in the gas-phase concentration, clean beds initially, and micropore diffusion control:

$$\frac{Q_t}{Q_\infty} = \frac{6}{\sqrt{\pi}} \cdot \sqrt{\frac{D}{r^2} \cdot t}$$

Where Q_t is the gas uptake at time t, Q_∞ is the gas uptake at equilibrium, D is the diffusivity and r is the radius of the equivalent spherical particle. The slopes of Q_t/Q_∞ versus $\sqrt{t}$ are derived from the fitting of the plots in the low gas uptake range.

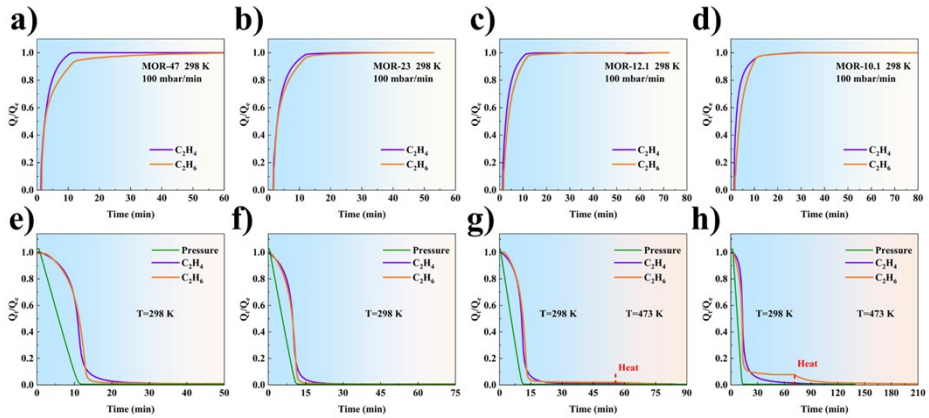

Fig. S14. (a-d) Adsorption kinetic and (e-h) desorption behaviors of MOR-47, 23, 12.1, and 10.1.

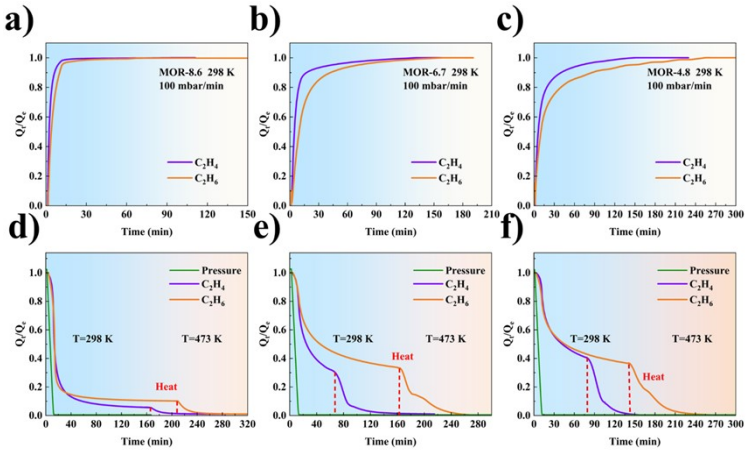

Fig. S15. (a-c) Adsorption kinetic and (d-f) desorption behaviors of MOR-8.6, 6.7, and 4.8.

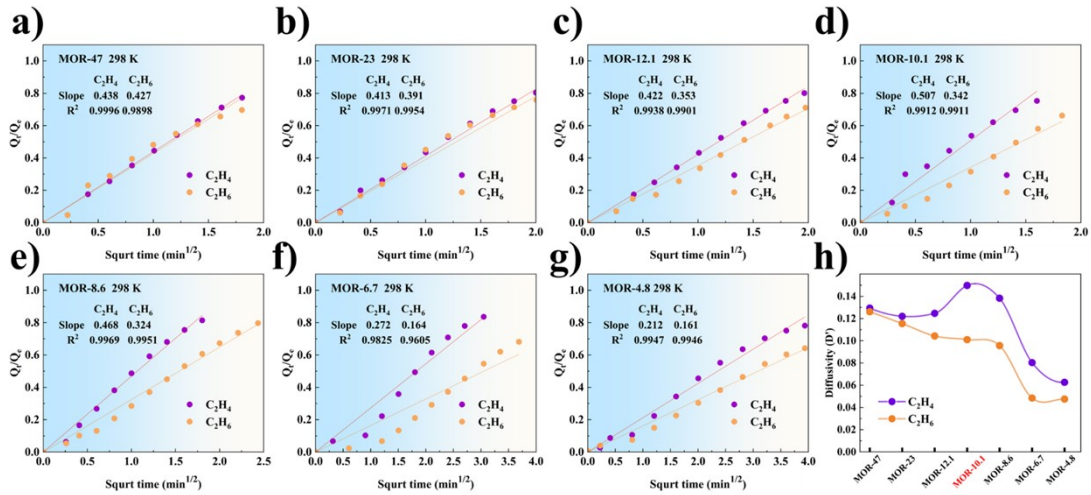

Fig. S16. Diffusional time constant calculation details for MOR-*x* at 298 K.

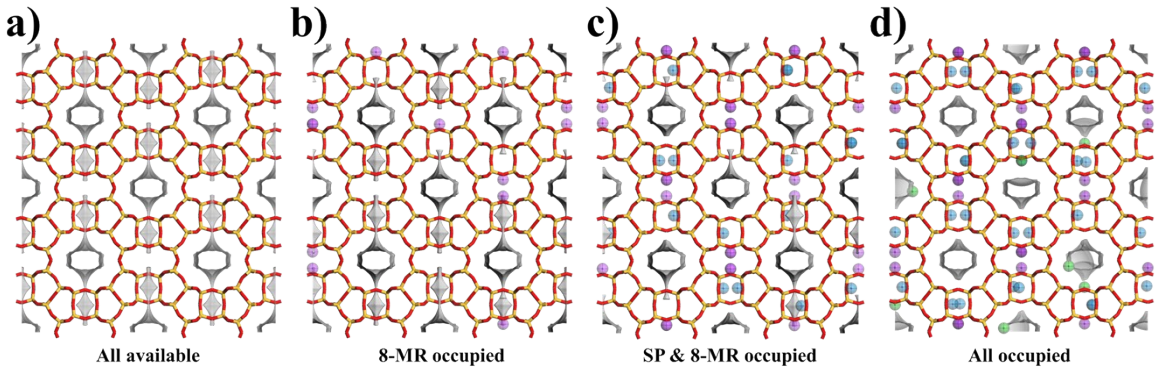

Fig. S17. (a-d) Accessible space in MOR with different Si/Al (pure-silica, 2 Na^+/U.C, 4 Na^+/U.C, and 6 Na^+/U.C.).

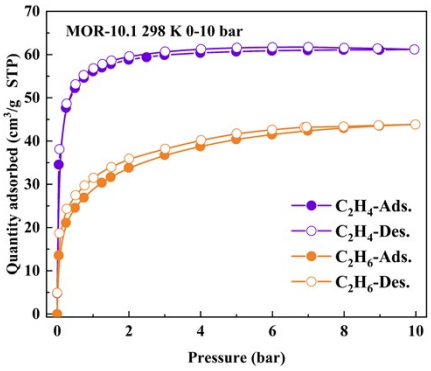

Fig. S18. High pressure adsorption isotherm of C_2H_4 and C_2H_6 of MOR-10.1.

Separation Experiment

All mixture gases were provided by Jining XieLi Special Gas Co., Ltd.

Table S4. Detection of gases

Gas	Detection sensitivity	Carrier gas
C_2H_4	10 ppm	Helium
C_2H_6	10 ppm	Helium
N_2	100 ppm	Argon

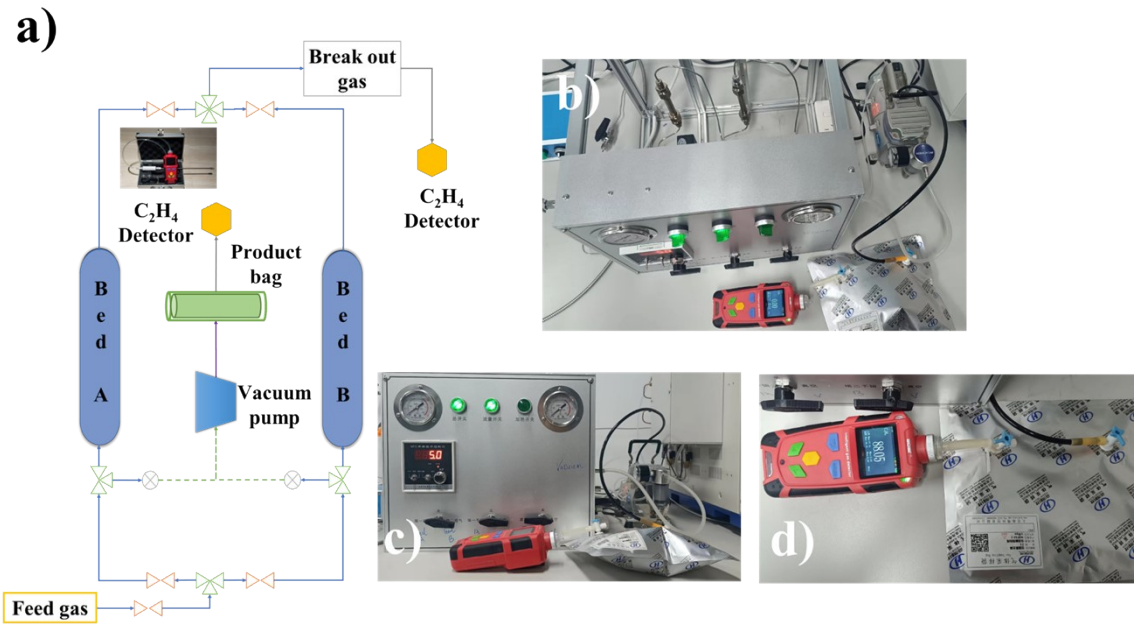

Fig. S19. (a) Scheme of mini-VPSA setup, (b-d) Photos of setup.

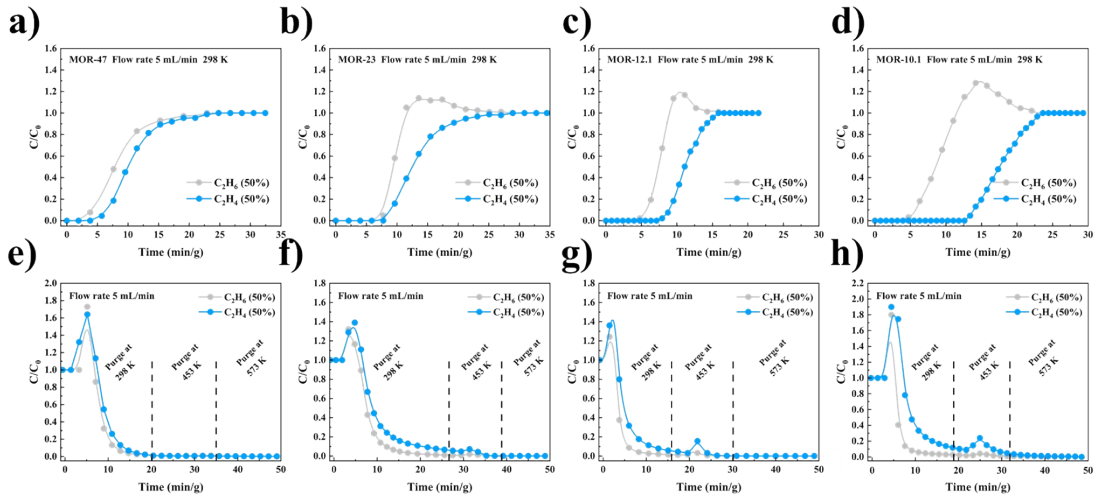

Fig. S20. C_2H_4/C_2H_6 (50/50, v/v) breakthrough experiments of MOR-47, 23, 12.1, and 10.1.

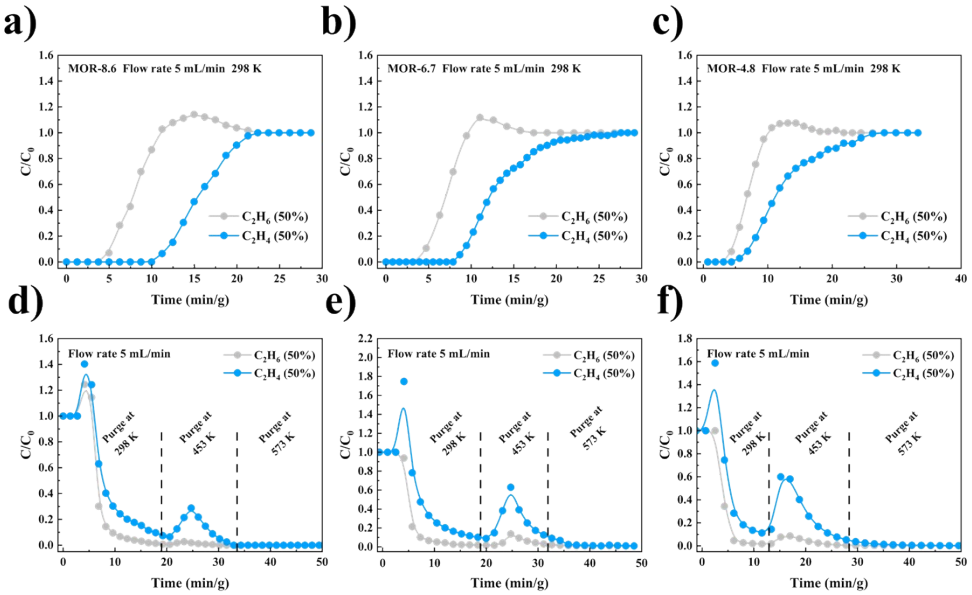

Fig. S21. C_2H_4/C_2H_6 (50/50, v/v) breakthrough experiments of MOR-8.6, 6.7, and 4.8.

Table S5. Dynamic uptake of MOR-*x*.

No.	C_2H_4 dynamic uptake (mmol g^{-1})	C_2H_4 in each super cell	C_2H_6 dynamic uptake (mmol g^{-1})	C_2H_6 in each super cell
Pure silica	Blank control	30	Blank control	30
MOR-47	1.20	28	0.95	22
MOR-23	1.27	29	0.93	21
MOR-12.1	1.38	32	0.75	17
MOR-10.1	1.98	47	0.61	15
MOR-8.6	1.89	45	0.76	16
MOR-6.5	1.48	35	0.72	17
MOR-4.8	1.40	34	0.70	17

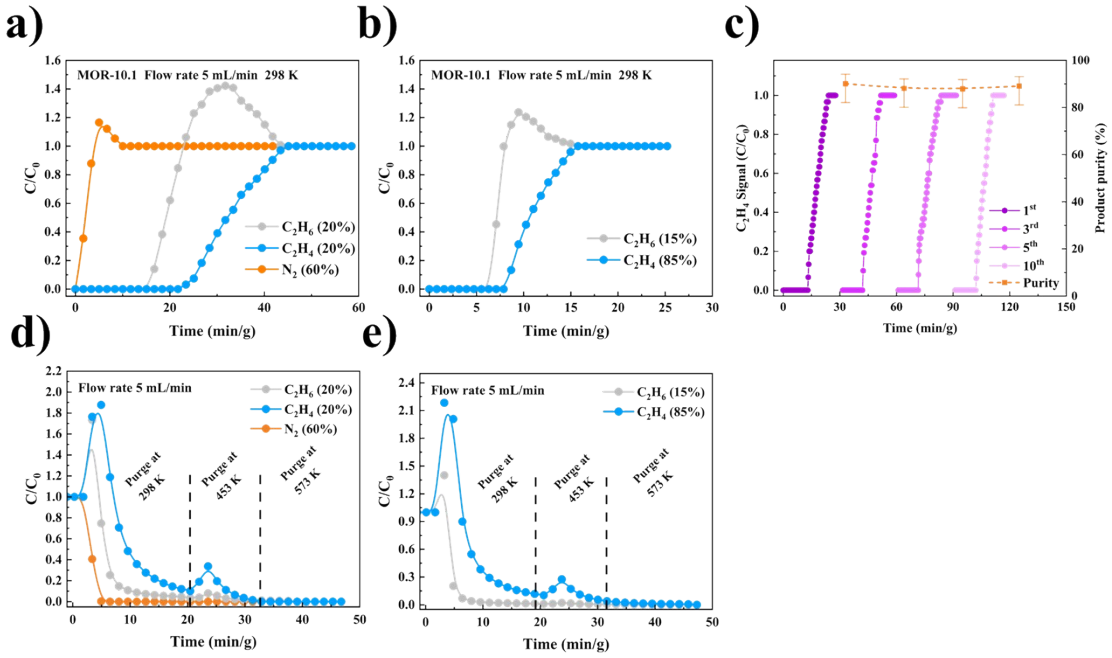

Fig. S22. (a, d) $C_2H_4/C_2H_6/N_2$ (20/20/60, v/v/v) and (b, e) C_2H_4/C_2H_6 (85/15, v/v) breakthrough experiments of MOR-10.1, (c) separation performance of MOR-10.1 in mini-VPSA process.

Sample stability characterization

Samples were exposed to air, different **pH** levels, and organic solvents, and their structural integrity was tested using **XRD**. Adsorption properties were analyzed using ASAP 2020. The air stability of samples is determined by exposing them to the air for different periods of time. Some organic solvents such as dimethylformamide, toluene, and carbon tetrachloride are used to explore stability. Sample (1 g) was added to a 50 mL solution and stirred for 48 hours. **pH** levels were adjusted by varying concentrations of NaOH and HNO_3. Prior to evaluate the structural integrity and the adsorption properties, the samples underwent ion exchange using a NaCl solution (1 mol/L, 50 mL) at 353 K for 8 hours with stirring to account for changes in equilibrium ions caused by **pH** variation.

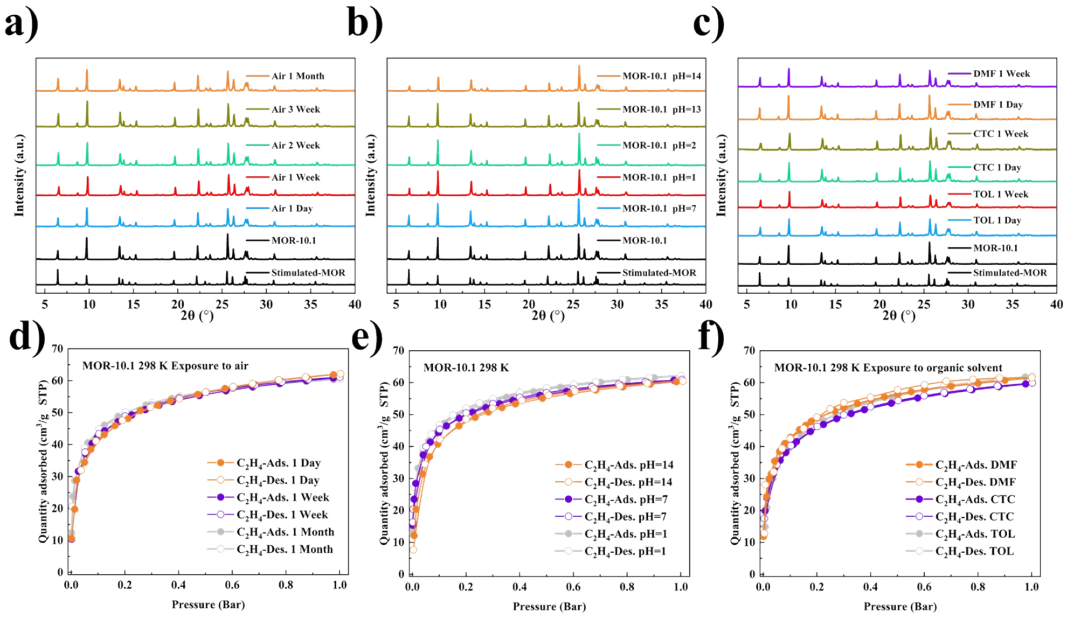

Fig. S23. (a-c) XRD patterns of MOR-10.1 exposed to air, different pH, and organic solvents, (d-f) adsorption isotherms of C_2H_4.

Details of Stimulation

The **GCMC** simulations were conducted to determine the location of Na^+ cations in **MOR**. The framework were treated as rigid, and the fixed loading task and metropolis method were employed to simulate optimal adsorption sites at 298 K and 1.0 bar. The loading steps, equilibration steps, and production steps were all set to 1.0×10^7. The interactions between the skeleton and guest molecules were characterized using the **COMPASS II** force field, and guest gas molecules were optimized using the **DMol3** module. The reported energy represents the minimum energy state of a structure containing one Al atom (and one Na^+ cation) per unit cell, and the minimum energy state corresponds to the most favorable location for the cations, indicate that the order of site occupancy obtained by all methods is as follows: T3 > T4 > T1 > T2[8-10]. To ensure a fair comparison, the super unit cells (222) based on the experimental Si/Al ratio were built. Simulations were carried out for the same partial pressure of C_2H_4 and C_2H_6 in pure Si-**MOR** as blank control. As for the effects of host-guest interaction, we use the calculation energy result based on the MS software:

$$E_{int} = E_{A-B} - (E_A + E_B)$$

E_{A-B} is the total energy for the A-B combination, E_i is the energy for the structure i.

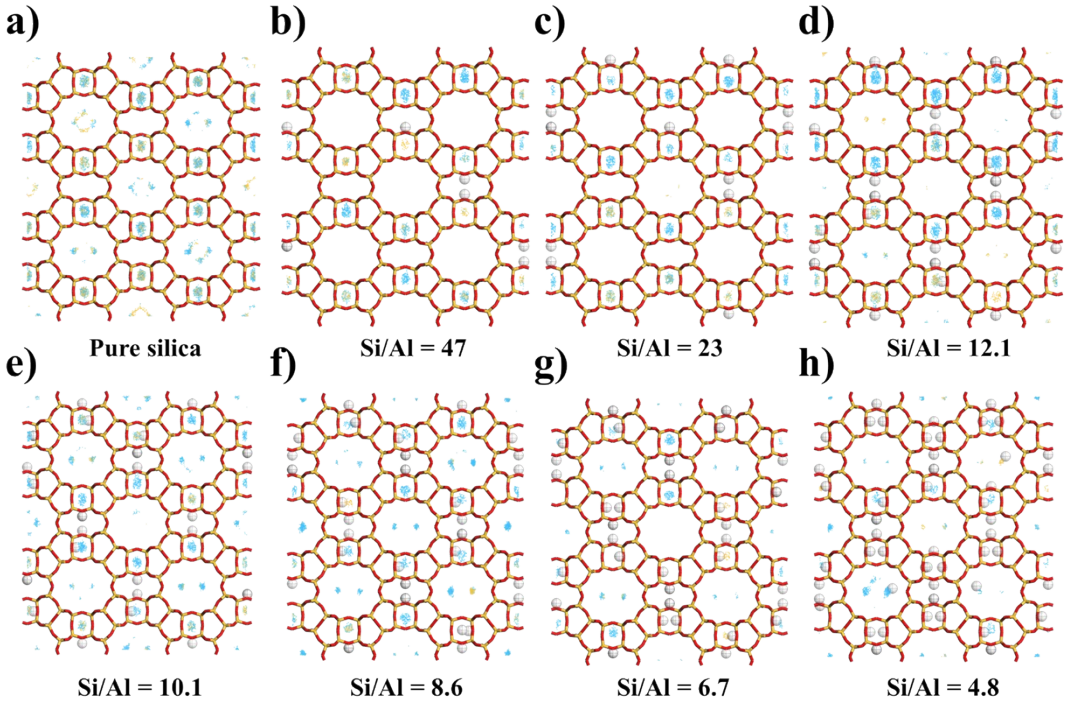

Fig. S24. Density distribution of C_2H_4 (blue), and C_2H_6 (orange) under the loading calculated from (a) blank control, and (b-h) breakthrough experiments.

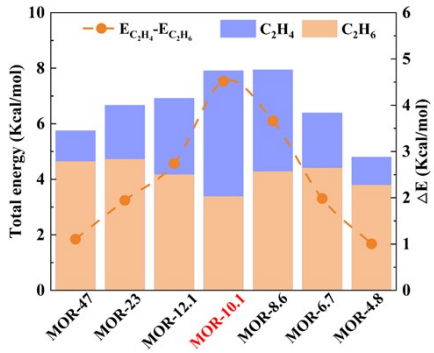

Fig. S25. C_2H_4 and C_2H_6 host-guest interaction energy simulation.

Reference

1. P. J. Bereciartua, A. Cantin, A. Corma, J. L. Jorda, M. Palomino, F. Rey, S. Valencia, E. W. Corcoran, Jr., P. Kortunov, P. I. Ravikovitch, A. Burton, C. Yoon, Y. Wang, C. Paur, J. Guzman, A. R. Bishop and G. L. Casty, Control of zeolite framework flexibility and pore topology for separation of ethane and ethylene, *Science*, 2017, **358**, 1068-1071.
2. M. Shi, C. C. H. Lin, T. M. Kuznicki, Z. Hashisho and S. M. Kuznicki, Separation of a binary mixture of ethylene and ethane by adsorption on Na-ETS-10, *Chem. Eng. Sci.*, 2010, **65**, 3494-3498.

3. L. Yu, W. Chu, S. Z. Luo, J. D. Xing and F. L. Jing, Experimental Study of Silver-Loaded Mesoporous Silica for the Separation of Ethylene and Ethane, *J. Chem. Eng. Data*, 2017, **62**, 2562-2569.
4. L. Chen and X. Q. Liu, π-complexation mesoporous adsorbents Cu-MCM-48 for ethylene-ethane separation, *Chinese J. Chem. Eng.*, 2008, **16**, 570-574.
5. F. Gao, Y. Q. Wang, X. Wang and S. H. Wang, Adsorptive separation of ethylene/ethane mixtures with CuCl@HY adsorbent: equilibrium and reversibility, *J. Porous Mat.*, 2017, **24**, 713-719.
6. A. Van Miltenburg, W. Zhu, F. Kapteijn and J. A. Moulijn, Adsorptive Separation of Light Olefin/Paraffin Mixtures, *Chem. Eng. Res. Des.*, 2006, **84**, 350-354.
7. N. Hedin, G. J. DeMartin, W. J. Roth, K. G. Strohmaier and S. C. Reyes, PFG NMR self-diffusion of small hydrocarbons in high silica DDR, CHA and LTA structures, *Micropor. Mesopor. Mat.*, 2008, **109**, 327-334.
8. M. Jeffroy, C. Nieto-Draghi and A. Boutin, New Molecular Simulation Method To Determine Both Aluminum and Cation Location in Cationic Zeolites, *Chem. Mater.*, 2017, **29**, 513-523.
9. A. Vjunov, J. L. Fulton, T. Huthwelker, S. Pin, D. Mei, G. K. Schenter, N. Govind, D. M. Camaioni, J. Z. Hu and J. A. Lercher, Quantitatively probing the Al distribution in zeolites, *J. Am. Chem. Soc.*, 2014, **136**, 8296-8306.
10. B. Liu, E. García-Pérez, D. Dubbeldam, B. Smit and S. Calero, Understanding Aluminum Location and Non-framework Ions Effects on Alkane Adsorption in Aluminosilicates: A Molecular Simulation Study, *J. Phys. Chem. C*, 2007, **111**, 10419-10426.